Atmos. Chem. Phys. Discuss., https://doi.org/10.5194/acp-2018-76
Manuscript under review for journal Atmos. Chem. Phys.
Discussion started: 16 April 2018

Atmospheric Chemistry and Physics Discussions

Modeling tropospheric O_3 evolution during the 2016 Group of Twenty summit in Hangzhou, China

Zhi-zhen Ni[1], Kun Luo[1*], Yang Gao[2], Fei Jiang[3], Xiang Gao[1], Jian-ren Fan[1], Chang-hong Chen[4]

[1]State Key Laboratory of Clean Energy, Department of Energy Engineering, Zhejiang University, Hangzhou 310027, China

[2] Key Laboratory of Marine Environment and Ecology, Ministry of Education of China, Ocean University of China, Qingdao 266100, China

[3]International Institute for Earth System Science, Nanjing University, Nanjing, China

[4]Shanghai Academy of Environmental Sciences, Shanghai 200233, China

Submitted to

Atmospheric Chemistry and Physics

[*]Corresponding author: State Key Laboratory of Clean Energy Utilization, Institute for Thermal Power Engineering of Zhejiang University, NO. 38 Zheda Road, Hangzhou 310027, P. R. China

E-mail address: zjulk@zju.edu.cn; Tel/Fax: 86-571-87951764

Atmos. Chem. Phys. Discuss., https://doi.org/10.5194/acp-2018-76
Manuscript under review for journal Atmos. Chem. Phys.
Discussion started: 16 April 2018

Atmospheric Chemistry and Physics Discussions

Abstract: To elucidate the factors governing the urban O_3 pollution during the campaign period of 2016 Group of Twenty (G20) summit in China, the Weather Research Forecast with Chemistry (WRF-Chem) model was used to simulate the spatial and temporal O_3 evolution in the Yangtze River Delta (YRD) region from August 24 to September 06, 2016. A unique mechanism was found to modulate the high ozone episodic event. Before the tropical cyclone, a prevailing north wind component brought in emission sources which are favorable for ozone formation. With the invasion of tropical cycle, subsidence air and stagnant weather were induced. Together with local urban heat island effect, there factors intensify ozone pollution in the YRD region. Different atmospheric processes were further analyzed to investigate the control factors of ozone formation through the integrated process rate method. It was found that both the vertical diffusion and the enhancing process of local chemical generation accounted for the growth of surface O_3 concentration in Hangzhou. Besides, dynamical circulations of O_3 advection associated with urban heat island effect were observed during the high O_3 episode (August 24–25, 2016), and low O_3 episode on September 5–6, 2016 was mainly resulting from the local chemical consumption. This provides insight into urban O_3 formation and dispersion in East China during the tropical cyclone events.

Keywords: Ozone, Tropical cyclone, WRF-Chem, Process analysis, Air quality

Atmos. Chem. Phys. Discuss., https://doi.org/10.5194/acp-2018-76
Manuscript under review for journal Atmos. Chem. Phys.
Discussion started: 16 April 2018

1. Introduction

Tropospheric O_3 is generated by a series of photochemical reactions involving volatile organic compounds (VOCs), nitrogen oxides (NO_x), and CO. Severe O_3 pollution usually occurs with the presence of sunlight, unfavorable meteorological conditions, and abundant O_3 precursors (Wang et al., 2006). As a primary ingredient in photochemical smog, ground-level O_3 pollution not only has detrimental effects on human health (Ha et al., 2014; Kheirbek et al., 2013) and the ecosystem (Landry et al., 2013; Teixeira et al., 2011) but also has warming effects as a short-lived climate forcer (Monks et al., 2015). The contribution of outdoor air pollution sources to premature mortality could be increasing globaly in the coming decades (Lelieveld et al., 2015). In Europe, 98% of the urban population is exposed to O_3 concentrations exceeding those reported in the World Health Organization Air Quality Guideline from 2010 to 2012 (Ortiz, 2015). O_3 levels in the United States of America (USA) and European cities are increasing more than at rural sites, while peak values are decreasing during 1990-2010 (Paoletti et al., 2014). Nagashima et al., (2017) states long-term (1980–2005) increasing trend in surface O_3 over Japan is mainly explained as the sum of trends in contributions of other regions (paticularly from China) to photochemical O_3 production. In addition, urban O_3 pollution events can also be observed in developing countries, such as Thailand (Zhang and Kim Oanh, 2002) and India (Calfapietra et al., 2016).

Recent years in China, air quality is deteriorating with the evolving urbanization and motorization. Many field and modeling studies have been conducted to investigate the photochemical characteristics of near-surface O_3 (Tang et al., 2009, 2012; Wang et al., 2013, 2014), photochemistry of O_3 and its precursors (Xie et al., 2014), interactions of O_3 with $PM_{2.5}$ (Shi et al., 2015), and urban O_3 formation (Tie et al., 2013). In addition to anthropogenic emissions of O_3 precursors, uncontrollable meteorology is an important factor modulating changes in O_3 concentration, through atmospheric physical and chemical processes (Xue et al., 2014). O_3 concentrations over the Yangtze River Delta (YRD) region, China were mainly contributed by the transport and diffusion from surrounding areas (Gao et al. 2016; Jiang et al. (2012). Synoptic

patterns related to tropical cyclones may be optimal weather conditions conducive to this high O_3 concentrations (Huang et al., 2005). Jiang et al., (2015) states the enhancement of stratosphere–troposphere exchange (STE) driven by a tropical cyclone, abruptly increased O_3 (21–42 ppb) in the southeast China during June 12–14, 2014. STE has recently been highlighted to be a significant contributor to near-surface O_3 concentrations (Lin et al. 2012; Lin et al., 2015). However, understanding the complex dynamics in atmospheric processes regarding O_3 formation, as well as identifying the main processes accounting for high O_3 concentrations, is nontrivial due to the limited measurements. O_3 pollution characteristics and underlying causes, in particular over megacities, are still unclear, thus understanding the mechanism modulating O_3 variations is vital for pollution prevention.

In this study, we used a regional air quality model to elucidate the chemical and physical factors governing O_3 abundance during the Group of Twenty (G20) summit. This summit was held in Hangzhou, China to discuss the sustainable and healthy development of the world economy. Emergency emission control measures (e.g., industrial stoppages, vehicle-limiting movement, and artificial rainfall) have been implemented over an area with a diameter of approximately 600 km to improve the air quality from August 24 to September 6, 2016. With severe concerns regarding O_3 concentrations in Hangzhou, this episode of megacity O_3 pollution has attracted wide policy-related interest. The rest of this paper is organized as follows. Section 2 outlines the methodology of the model system and its configuration. Section 3 presents the synoptic weather conditions, O_3 formation-related individual atmospheric processes. Section 4 discusses the background O_3, transport patterns, and reasons for O_3 pollution in Hangzhou. Finally, Section 5 presents a summary of the findings.

2. Methodology

2.1. Regional chemistry modeling system

To understand the interactions among emissions, meteorology, and chemistry, the WRF-Chem model (Version 3.7) was used to simulate the temporal and spatial O_3 evolution. WRF-Chem is a

Atmos. Chem. Phys. Discuss., https://doi.org/10.5194/acp-2018-76
Manuscript under review for journal Atmos. Chem. Phys.
Discussion started: 16 April 2018

Atmospheric Chemistry and Physics Discussions

94 regional online-coupled air quality model that simultaneously simulates air quality components with
95 meteorological components by using identical transport schemes, grid structures, and physical
96 schemes (Grell et al., 2005). Two model domains were designed in this study (Fig. 1a), namely an
97 outer domain (horizontal resolution: 30 km), covering East China (20.0–44.5°N, 99.0–126.5°E),
98 and an inner domain (horizontal resolution: 6 km), covering the YRD region (27.6–32.7°N, 116.9–
99 122.4°E), with a "Lambert conformal conic" projection centered on Central China (34°N, 111°E).
100 The domains included a total of 31 vertical layers up to 100 hPa with finer vertical resolutions near
101 the surface. The simulation period was from August 17 to September 6, 2016, with the first week
102 simulations conducted to spin up the model; the hourly data during August 24–September 6,
103 corresponding to the official air pollution control measures implemented during the G20 summit,
104 were used in the following analysis. Other detailed information regarding the configuration of
105 WRF-Chem model has been described by our previous study (Ni et al., 2018).

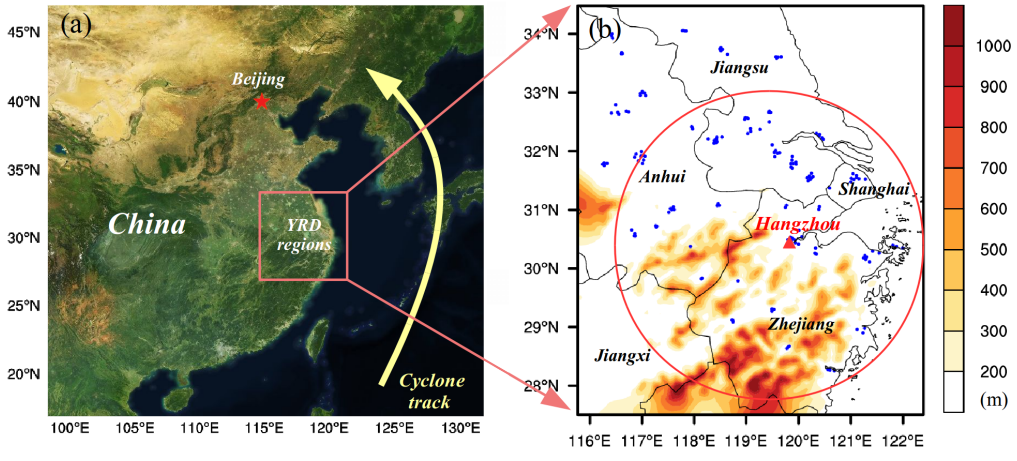

106 **Fig. 1.** Double-nested simulation domains. (a) Domain 1: 30 km in East China with 102 (W–E) × 111 (S–N) × 31
107 (vertical layers) grids; Domain 2: 6 km in the Yangtze River Delta (YRD) region with 100 (W–E) × 115 (S–N) ×
108 31 (vertical layers) grids. (b) Color bar (right) represents the terrain elevations. Blue dots denote the air quality
109 monitoring sites. The red circle represents the control scales of emission control measures.

110 Geographical data, including terrain elevations (Fig. 1b), soil properties, and albedo, were
111 primarily interpolated from the United States Geological Survey database (Brown et al., 1993).
112 Land surface parameters, including land use categories, green vegetation fraction, and leaf area

index were specified by applying the Moderate-Resolution Imaging Spectroradiometer (MODIS) satellite observations (Friedl et al., 2002; Li et al., 2014). The meteorological boundary and initial conditions were determined from the global objective final analysis (FNL) data of the National Centers for Environmental Prediction. The FNL data were also assimilated to domain 1 (East China) by using the grid-nudging method (Stauffer et al., 1991) to reduce the meteorological integral errors. Furthermore, the chemical boundary and initial conditions were interpolated from the results of the global Model for Ozone and Related Chemical Tracers Version 4 (MOZART4) (Emmons et al., 2010).

2.2. Emissions

As crucial model inputs, primary anthropogenic emissions included species of SO_2, NO_x, CO, NH_3, $PM_{2.5}$, and VOCs, mainly from several sectors including the power, industrial, residential, transportation, and agricultural sectors. The monthly Multiresolution Emission Inventory for China (MEIC, 0.25°× 0.25°; http://www.meicmodel.org/) was used for domain 1 in East China (Li et al., 2017). Custom finer emission inventories in Hangzhou were used for domain 2 in the YRD region, in accordance with the policies of emission control strategies implemented. The emission inventories for the two domains were projected into horizontal and vertical gridded-hourly emissions with temporal and vertical profiles obtained from Wang et al. (2011). VOCs emissions were categorized into modeled species, according to von Schneidemesser et al. (2016). Biogenic emissions were generated using the Model of Emission of Gases and Aerosols from Nature (Guenther et al., 2006). Dust emissions were calculated online from surface features and meteorological fields by using the Air Force Weather Agency and Atmospheric and Environmental Research scheme (Jones et al., 2011). Other uncontrollable or small amounts of emissions (i.e., biomass burning, aviation, and sailing ship) were not considered in this particular period.

2.3. Integrated process rate analysis

To understand the mechanism underlying O_3 formation, individual physical and chemical processes of O_3 formation were investigated using integrated process rate (IPR) analysis

incorporated into the WRF-Chem model. IPR analysis has been widely applied and proven to be an effective tool for demonstrating the relative importance of individual processes and providing a fundamental interpretation of O_3 concentrations (Goncalves et al., 2009; Tang et al., 2017; Shu et al., 2016). In this study, atmospheric processes of O_3 formation, including gas chemistry, vertical diffusion, and horizontal and vertical advection, were investigated. Other processes (i.e., cloud process and horizontal diffusion) that either play minor roles or act as a sink (i.e., dry and wet deposition) were not presented in this study.

2.4. Evaluation method

To gain confidence in model result interpretation, the first step is to evaluate model outputs based on observations. Accordingly, in this study, the model results derived from domain 2 were compared with hourly surface observational data obtained from 96 air quality monitoring sites in the YRD regions (blue dots, Fig. 1b). The air pollutants included O_3 and NO_2. Model performance was evaluated using statistical measures, namely mean fractional bias (MFB) and mean fractional error (MFE) and correlation coefficient (R), with formula shown in Table S1, following the recommendation of the US Environmental Protection Agency (US EPA; 2007). Additionally, the meteorological parameters included temperature at 2 m (T2), relative humidity at 2 m (RH2), and 10-m wind speed (WS10) and direction (WD10). Commonly used mean bias (MB), gross error (GE), and root mean square error (RMSE), with equations shown in Table S1, were calculated as the statistical indicators, according to the study of Zhang et al. (2014).

The vertical distribution of modeled O_3 in Hangzhou was evaluated by conducting comparisons with the observed differential absorption LiDAR (DIAL) data. In the DIAL technique, the mean gas concentration over a certain range interval is determined by analyzing the LiDAR backscatter signals for laser wavelengths tuned "on" (λ_{on}) and "off" (λ_{off}) a molecular absorption peak of the gas under investigation (Browell et al., 1998). The application of the DIAL technique measurement of O_3 concentrations above or around a specific location (Browell, 1989). In our

Atmos. Chem. Phys. Discuss., https://doi.org/10.5194/acp-2018-76
Manuscript under review for journal Atmos. Chem. Phys.
Discussion started: 16 April 2018

Atmospheric Chemistry and Physics Discussions

164 DIAL datasets, the available vertical height ranged only from 0.3 to 3 km, because of the limitation
165 of the signal-to-noise ratio and detection range.

166 ## 3. Results

167 ### 3.1. Model performance evaluation

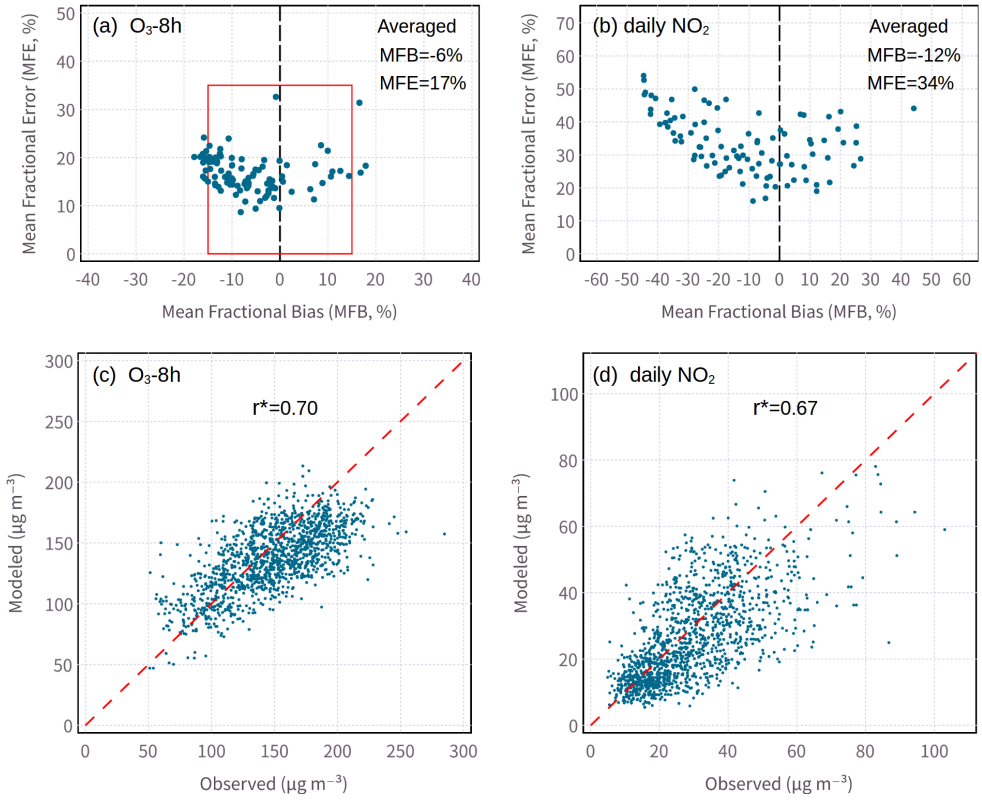

168

169 **Fig. 2.** Statistical performance of the modeled and observed concentrations of the air pollutants from 96 air quality
170 monitoring sites over YRD from August 24 to September 6, 2016 (1,344 daily pairs). Mean fractional bias (MFB)
171 and mean fractional error (MFE) for (a) O_3-8h and (b) daily mean NO_2. (Each point denotes a site). Performance
172 goals (red box) for O_3 are the benchmarks. Correlation coefficient (r) for (c) O_3-8h and (d) daily mean NO_2. (Each
173 point denotes a daily pair).

174 We first evaluate the overall performance of WRF-Chem over the YRD region by
175 incorporating the 96 air quality monitoring sites. The maximum daily 8-hr (O_3-8h) ozone and daily
176 mean NO_2 at surface were used. The model-simulated air pollutants in general agree with the
177 observations, shown in Fig. 2. The mean MFB and MFE O_3-8h was -6%, 17%, respectively (Figs.

Atmos. Chem. Phys. Discuss., https://doi.org/10.5194/acp-2018-76
Manuscript under review for journal Atmos. Chem. Phys.
Discussion started: 16 April 2018

Atmospheric Chemistry and Physics Discussions

178 2a and c), within the benchmarks (MFB: 15% and MFE: 35%) proposed by the US Environmental
179 Protection Agency (US EPA; 2007). The daily mean NO_2 level also achieved a reasonable
180 performance, with MFB of -12%, MFE of 34% (Figs. 2b and d). Both the simulated O_3 (Pearson r
181 of 0.70) and NO_2 (Pearson r of 0.67) shows statistically significant correlation with the observed
182 data at the 95% level. The performance in this study is comparable to the previous studies (Tuccella
183 et al., 2012; Zhang et al., 2016).

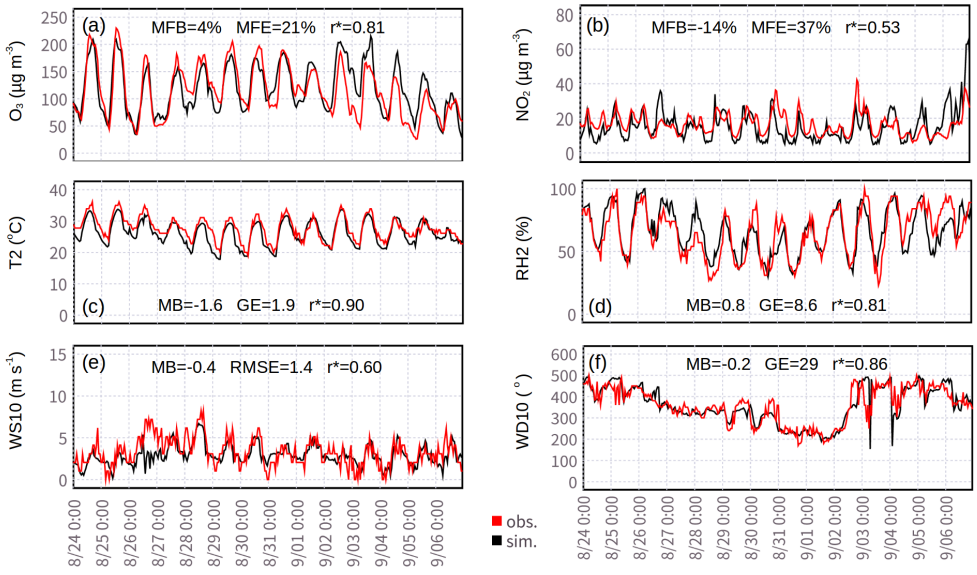

184 **Fig. 3.** Statistical performance of the modeled and observed air pollutants and meteorological parameters in
185 Hangzhou from August 24 to September 6, 2016. Surface concentrations of O_3 and NO_2, temperature at 2 m (T2),
186 relative humidity at 2 m (RH2), wind speed at 10 m (WS10) and wind direction at 10 m (WD10). All modeled
187 data shows statistically significant correlation with the observed data at the 95% level

188 Following the overall evaluation over YRD above, the site of Hangzhou was zoomed in to
189 elucidate the ability of WRF-Chem in reproducing the air quality and meteorological conditions.
190 Time series of hourly simulated and observed air pollutants (O_3, Fig. 3a; NO_2, Fig. 3b) and
191 meteorology (2-meter air temperature: T2, Fig. 3c; 2-meter relative humidity: RH2, Fig. 3d; 10-
192 meter wind speed: WS10, Fig. 3e and 10-meter wind direction: WD10, Fig. 3f) were shown in Fig.
193 3. The observed diurnal variations were in general well captured by WRF-Chem. For example, the

Atmos. Chem. Phys. Discuss., https://doi.org/10.5194/acp-2018-76
Manuscript under review for journal Atmos. Chem. Phys.
Discussion started: 16 April 2018

Atmospheric Chemistry and Physics Discussions

194 MFB and MFE for both O_3 and NO_2 was close to benchmark in particular of O_3 (MFB/MFE:
195 4%/21%), well below the standard (MFB/MFE: 15%/35%) (US EPA; 2007).

196 For meteorological parameter evaluation, Emery et al. (2001) proposed benchmarks, including
197 2-meter air temperature (MB ≤ ± 0.5 ºC, GE ≤ 2.0 ºC), 10-meter wind speed (MB ≤ 0.5 m/s, RMSE
198 ≤ 2.0 m/s) and 10-meter wind direction (MB ≤ ± 10 deg, GE ≤ 30 deg). McNally (2009) indicated a
199 relaxed benchmark for 2-mter temperature (MB ≤ ± 1.0 ºC). The10-meter wind speed and wind
200 direction is well within the criteria. The GE of 2-mter air temperature (1.9 ºC) also satisfies the
201 criteria, albeit the mean bias is slightly higher (-1.6 ºC), and the slightly higher temperature bias
202 occurs in the previously study as well (Zhang et al., 2014). Overall, the meteorological parameter
203 yields good performance in comparison to observations.

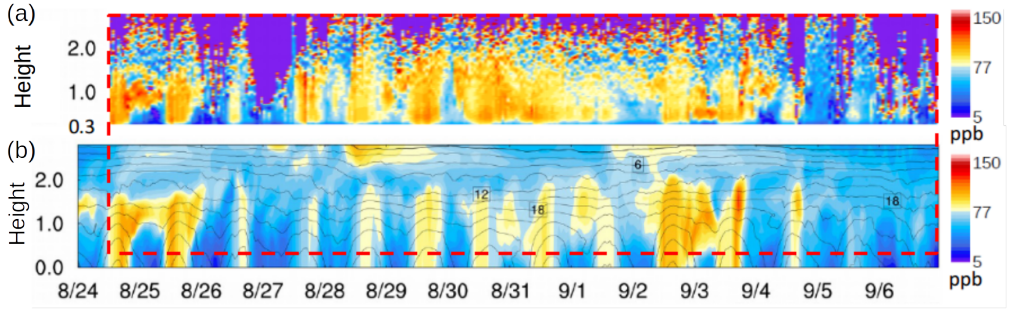

204 Fig. 4. Upper-level comparison of hourly (a) observed (from differential absorption lidar) and (b) simulated O_3
205 concentrations (ppb) in Hangzhou from August 24 to September 6, 2016. Purple regions in the top panel denote
206 the invalid data with a low signal-to-noise ratio. For an easy direct comparison, the red dashed line indicates the
207 ozone level at exactly the same time period (starting from 12:00, August 24) and vertical heights (0.3–3 km)
208 between the observations and simulation results.

209 To further delve into the ability of model in reproducing the vertical structure of ozone
210 concentration, a qualitative comparison of the vertical distribution between the modeled O_3 against
211 the DIAL datasets was shown in Fig. 4, depicting good consistency between model and observation.
212 Diurnal O_3 variations were observed mainly within the planetary boundary layer (approximately < 2
213 km). Notably, the model successfully captured a nocturnal O_3-rich mass, which exhibited an n-
214 shaped distribution in the upper air (approximately 1 km) on August 24, 2016, thus indicating that
215 the promising applicability of the model to pollution monitoring. Occasionally, the model revealed a

Atmos. Chem. Phys. Discuss., https://doi.org/10.5194/acp-2018-76
Manuscript under review for journal Atmos. Chem. Phys.
Discussion started: 16 April 2018

Atmospheric Chemistry and Physics Discussions

high O_3-rich mass (>90 ppb) at a height of approximately 3 km (nearly 700-hPa) i.e., on August 29 and September 2, 2016; however, no valid observed data could be used considering the low signal-to-noise ratio.

3.2. Synoptic weather system

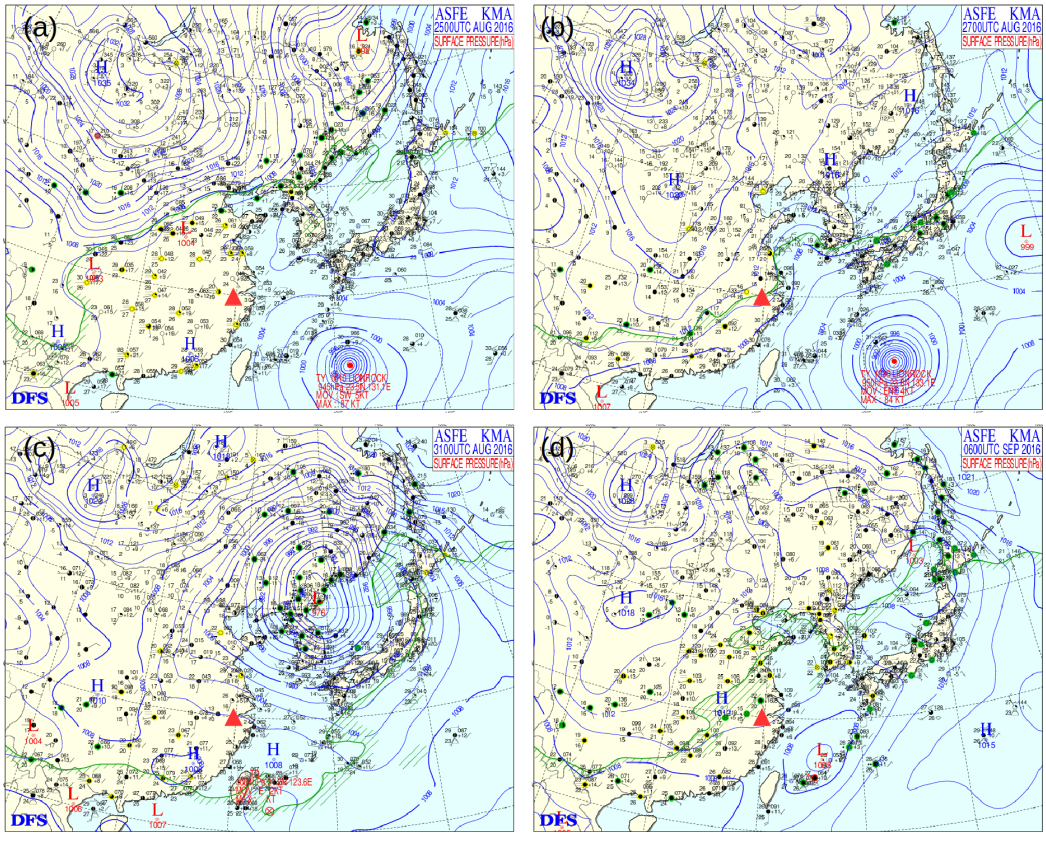

Fig. 5. Tropical cyclone evolution in East Asia during the 2016 G20 summit. Weather charts for four representative periods at 08:00 LST on (a) August 25, (b) August 27, (c) August 31, (d) September 6, 2016. LST: Local Sidereal Time; H: High-pressure system; L: Low-pressure system. The red triangle denotes the location of Hangzhou.

Because synoptic circulation is closely related to O_3 abundance, four representative surface weather charts obtained from the Korea Meteorological Administration were used to track the tropical cyclone (Fig. 5). In the early stage of the tropical cyclone during August 24–25, 2016 (Fig. 5a), strong uniform high-pressure fields covered vast regions of southeastern China. A tropical cyclone moved northeastward in the East China Sea. In the middle stage (Fig. 5b), the tropical

Atmos. Chem. Phys. Discuss., https://doi.org/10.5194/acp-2018-76
Manuscript under review for journal Atmos. Chem. Phys.
Discussion started: 16 April 2018

Atmospheric Chemistry and Physics Discussions

229 cyclone approached the YRD region and brought strong north wind fields. Notably, the long narrow
230 rain band arrived in Hangzhou (red triangle) on August 27, 2016. In the later stage (Fig. 5c), the
231 cyclone continually moved toward Japan on the following days and hit the land. Furthermore, the
232 tropical high in the YRD region recovered gradually. Finally, the cyclone faded, and a rainstorm
233 appeared in most of the YRD region. This rainstorm was sustained from almost September 2 to 7,
234 2016 (Fig. 5d, only the data for September 6 are presented for clarity).

235 **3.3. O_3 distribution at different heights**

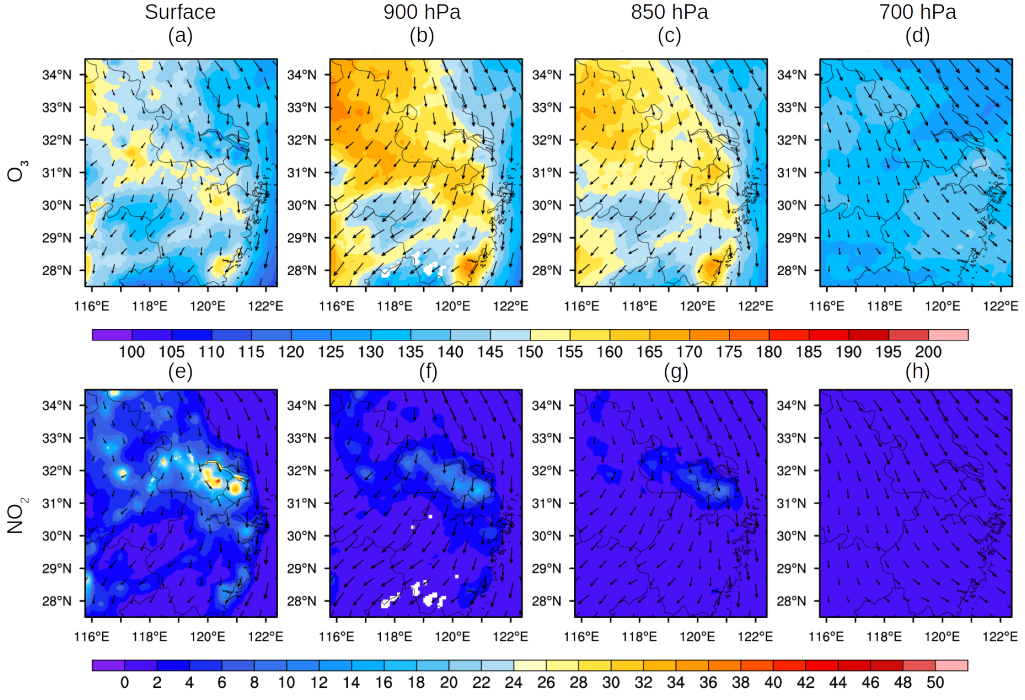

236 **Fig. 6.** Distribution of the simulated daytime mean concentrations of O_3 (08:00–17:00 LST on August 24–
237 September 6, 2016) and its precursor gas NO_x (shaded, μg m^{-3}) and wind fields (vector, m s^{-1}) in domain 2 at
238 several layers, as labeled on top of the plots.

239 The O_3 concentrations increased in the daytime. As illustrated in Fig. 6, the daytime mean
240 distributions of O_3 significantly varied at different vertical heights, with the dominant north wind
241 fields being from the surface to 700-hPa (approximately 3 km). On the surface (Fig. 6a), a relatively
242 high O_3 concentration (>150 μg m^{-3}) was found in Anhui province and the surrounding areas of
243 Hangzhou. By contrast, the O_3 concentrations were relatively low in mountainous areas, and south

of Jiangsu province (upwind regions of Hangzhou), which are industrial areas with high concentration of NO_2 (Fig. 6e). At 900-hPa, the O_3 concentrations (>150 μg m^{-3}, shown in yellow, Fig. 6b) were high in most of the YRD region, which were substantially higher than those at the ground level and 850-hPa layer. However, mountainous areas still had low O_3 concentrations, whereas those above the south of Jiangsu province notably had high O_3 concentrations. At 850-hPa (Fig. 6c), nearly on top of the planetary boundary layer (approximately 1.5 km), the O_3 distribution pattern was similar to that at 900-hPa; however, the O_3 concentrations at this level were lower because of the low concentrations of precursor gases. At 700-hPa (Fig. 6d), the O_3 distribution was less influenced by surface anthropogenic emissions. However, a notable background O_3 concentration was still uniformly distributed (nearly 140 μg m^{-3}). The concentrations of a precursor gas, NO_x, significantly decreased as the altitude increased (Figs. 6e–h), and NO_x was observed in trace amounts in the upper air. This result is in contrast to the O_3 variation found in the vertical layers.

3.4. O_3 pollution and transport patterns

Hourly vertical and horizontal O_3 distributions and wind fields in the YRD region are presented for three representative episodes (Fig. 7) according to the movement of the tropical cyclone. For stagnation days with weak wind fields (i.e., August 25 and September 2) before or after the tropical cyclone, meteorological conditions were unfavorable to pollutant dispersion. O_3 pollution was more regional and intense, with an hourly O_3 peak concentration of 250 μg m^{-3} at 14:00 LST below the high layer (1.5 km) around Hangzhou (Figs. 7a and f). For nighttime transport (Figs. 7b and c), a large O_3-poor mass (<30 μg m^{-3}) intruded downward. This nocturnal O_3-poor mass can be explained by the NOx-rich mass that consumed O_3 through titration reaction. Subsequently, at 14:00 LST (Fig. 7d), high O_3 concentrations appeared in the widespread region of south YRD (mountainous areas; Fig. 1b). By contrast, for daytime transport (Fig. 7e), a large belt of O_3-rich mass (>160 μg m^{-3}) appeared in the upwind direction and moved toward Hangzhou. Both of the described transport effects occurred under a prevailing north wind field. Fig. S1 shows the

Atmos. Chem. Phys. Discuss., https://doi.org/10.5194/acp-2018-76
Manuscript under review for journal Atmos. Chem. Phys.
Discussion started: 16 April 2018

Atmospheric Chemistry and Physics Discussions

270 corresponding patterns of NO_x. Besides, relevant atmospheric trajectories also support this transport
271 from North China (Fig. S2)

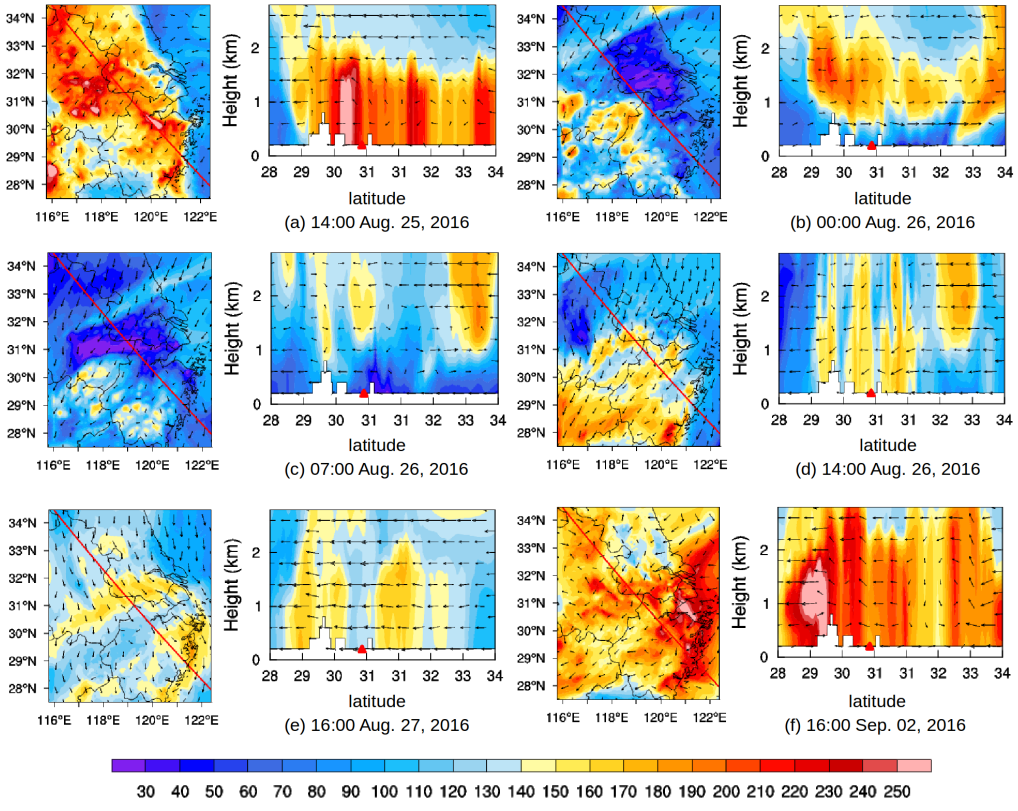

272 **Fig. 7.** Surface and upper-level O_3 distributions (μg m^{-3}) and wind fields (vectors, m s^{-1}) for representative
273 episodes. (a) Stagnant weather before the tropical cyclone, (b–e) pollutant transport when the tropical cyclone
274 approached, and (f) stagnant weather after the cyclone. The red line denotes the cross section line of upper-level
275 O_3 distributions. The red triangle denotes the location of Hangzhou.

276 **3.5. Process analysis of O_3 formation**

277 Four hourly modeled processes indicated the diurnal fluctuations in loops. Gas chemistry
278 generated O_3 nearly above the upper-air height of 2 km in the daytime but depleted O_3 at the near-
279 surface height (< 0.3 km) in the nighttime (Fig. 8a). O_3 from the upper layer diffused downward to
280 the ground through vertical diffusion during the study period but was significantly high in the
281 daytime (Fig. 8b). In addition, as presented in Figs. 8c and d, several O_3 dynamical circulations
282 were observed between the near-surface and upper-air heights, which were notable during August
283 24–25 and on September. 2, 2016. An O_3-rich mass in the lower layer (<1 km) traveled to

Atmos. Chem. Phys. Discuss., https://doi.org/10.5194/acp-2018-76
Manuscript under review for journal Atmos. Chem. Phys.
Discussion started: 16 April 2018

Atmospheric Chemistry and Physics Discussions

284 Hangzhou through horizontal advection, and it was transported from the upper layer to the high
285 layer (approximately 1.5 km) through vertical advection. The mass subsequently traveled out again
286 at the high layer through horizontal advection circularly. Urban heat island circulations caused the
287 upward and downward flows.

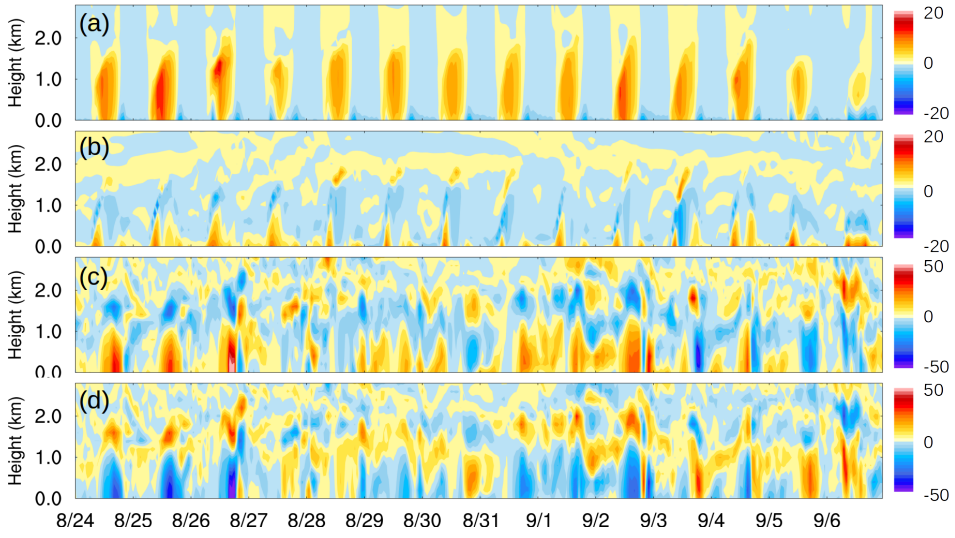

288 **Fig. 8.** Hourly variations in the change rate of upper-level O_3 (ppb/hour) because of (a) gas chemistry, (b) vertical
289 diffusion, (c) horizontal advection, and (d) vertical advection in Hangzhou.

290 Quantifying the daytime mean variations of O_3 at the ground level due to atmospheric
291 processes (Fig. 9a) revealed major positive contributions of gas chemistry, vertical diffusion, and
292 horizontal advection to surface O_3 formation, with mean production rates of 1.9, 3.3, and 6.7
293 ppb/hour, respectively, from August 24 to September 6, 2016. First, the trends between the daytime
294 mean values associated with gas chemistry and observed O_3-8h concentration were consistent (Fig.
295 9b), indicating the trade-off effect among vertical diffusion and horizontal and vertical advection.
296 High O_3 concentrations were accompanied by high gas chemical generation. Second, vertical
297 diffusion may compensate for gas chemistry to some extent when the chemical reaction rate is
298 relatively low or negative. For example, on August 26–27 and September 5–6, 2016, the vertical
299 diffusion rates were mostly greater than the chemical production rates. Finally, advection processes
300 were essential and integral components of air circulation, whereas horizontal advection exerted

Atmos. Chem. Phys. Discuss., https://doi.org/10.5194/acp-2018-76
Manuscript under review for journal Atmos. Chem. Phys.
Discussion started: 16 April 2018

Atmospheric Chemistry and Physics Discussions

301 remarkably positive effects on surface O_3 concentrations in Hangzhou and vertical advection
302 exerted dispersion effects.

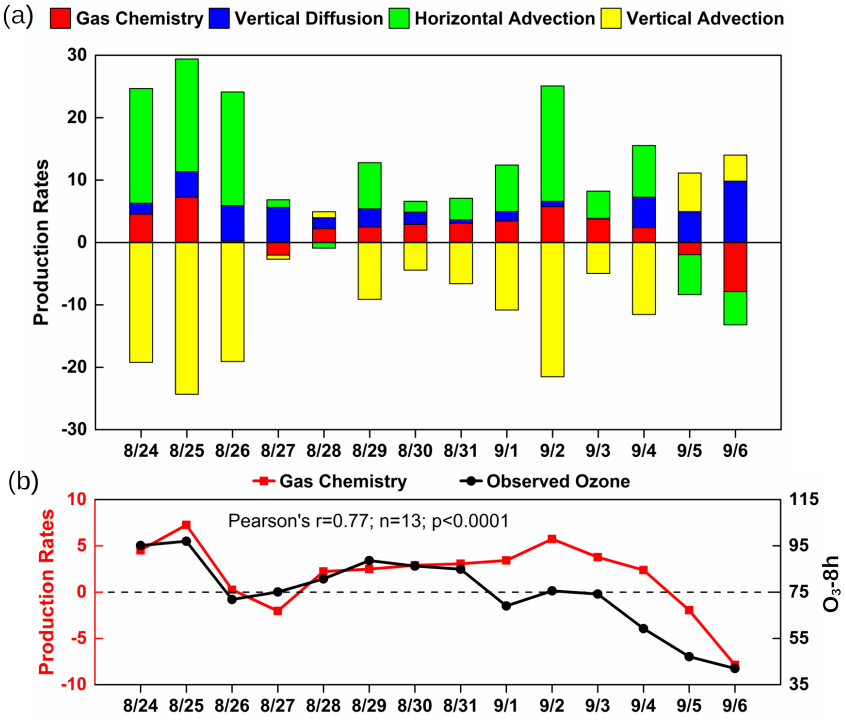

303 **Fig. 9.** (a) Daytime mean (08:00–17:00 LST) variations in simulated surface O_3 change rate (ppb/hour; left y axis)
304 because of gas chemistry, vertical diffusion, and horizontal and vertical advection in Hangzhou. (b) Comparison
305 of daytime mean gas chemistry generation (ppb/hour; left y axis) and observed surface maximum daily 8-hour
306 concentration of O_3 (O_3-8h; ppb; right y axis) in Hangzhou. China's national standard is approximately 75 ppb
307 (160 μg m^{-3}).

308 ## 4. Discussions

309 The results of this study reveal notable background O_3 concentrations in the upper-air layer in
310 the YRD region. O_3 concentrations were significantly higher at 900-hPa (approximately 1 km) than
311 at the surface, which is consistent with field study (Xing et al., 2017). This is probably because the
312 surface NO concentrations were still adequately high to consume O_3 through a titration reaction. By
313 contrast, at 900-hPa, the efficiency of O_3 photochemical production was highly nonlinear, with the
314 production rates being higher at lower NO_x levels (Zhang et al., 2008). This significant
315 concentration gradient explains the major downward vertical diffusion process. At 700-hPa

316 (approximately 3 km), the uniformly distributed O_3 (>130 μg m^{-3}) can be explained by the
317 concentration redistribution engendered by the diffusion process. Peripheral downdrafts in the
318 large-scale cyclone circulation can transport an extremely high O_3-rich mass in the upper
319 troposphere and lower stratosphere downward to the surface (Tang et al., 2011; Hsu and Prather,
320 2014). This O_3 intrusion was also reported in southeast China (Jiang et al., 2015). According to our
321 results, we can infer that a considerably high background O_3 concentration in the upper air may
322 markedly contribute to surface O_3 pollution, which is in agreement (hemispheric background) with
323 the findings of studies conducted in Europe (Wilson et al., 2012) and the United States (Lin et al.,
324 2012; 2015).

325 Our results demonstrate that Hangzhou experienced strong regional transport of pollutants
326 from North China on August 26–27, 2016. The transport was caused by a reinforced north wind
327 component because of the convergence of the tropical cyclone in East China Sea. This southward
328 transport of pollutants supplies raw materials for photochemical O_3 generation and explains the high
329 O_3 concentrations in the south of the YRD region, which comprises mountainous or scenic areas
330 with low anthropogenic emissions, despite the implementation of stringent emission control
331 measures. Our results suggest that more cooperation with upwind regions, such as North China, is
332 required to alleviate the potential transport of pollutants by tropical cyclones. Additional analysis
333 such as regional contributions to O_3 or its precursors in Hangzhou may yield quantitative evidence.

334 We demonstrate that the local chemical generation in Hangzhou was enhanced during episodes
335 of high O_3 concentrations before and after the tropical cyclone. Chemical generation of O_3 is the net
336 effect of photochemical generation and titration consumption. Oxidation reactions of VOCs, under
337 the present of CO, provide alternative oxidants (i.e., HO_2 and RO_2) that efficiently convert NO to
338 NO_2. This conversion enriches the reactants to O_3 photochemical generation while suppressing
339 titration consumption, resulting in the accumulation of O_3 (Jenkin et al., 1997; Sillman, 1999; Wang
340 et al., 2017). Downward shortwave flux at the ground level (Fig. S3) is more intense on days having
341 high O_3 concentrations than on those having low O_3 concentrations. This strong solar radiation

342 strengthens O_3 photochemical generation. In addition to the stagnant weather conditions, air
343 subsidence in peripheral circulations of tropical cyclones helps to trap heat and pollutants at the
344 surface (Jiang et al., 2015; Shu et al., 2016). Furthermore, a tropical system with calm hot–dry
345 weather favors the development of an urban heat island, which causes the thermal circulations and
346 converges the surrounding O_3 and its precursors (Lai and Cheng, 2009). Consequently, the
347 increased temperature also accelerates the photochemical reactions (Narumi et al., 2009; Walcek et
348 al., 1995). Therefore, enhanced photochemistry dominated the O_3 chemical generation, resulting in
349 high O_3 concentrations. This is consistent with field study (Su et al., 2017). By contrast, low-level
350 O_3 episodes (i.e., August 27 and September 6) in Hangzhou were determined to be accompanied by
351 a rain band in the YRD region. Rain-band-related cumulus clouds block solar radiation, thus
352 weakening O_3 photochemical generation. Therefore, titration consumption dominated the chemical
353 generation process, resulting in low or negative O_3 chemical production.

354 ## 5. Conclusions

355 O_3 evolution in Hangzhou during the G20 summit was well represented using the WRF-Chem
356 model. Statistical evaluation in meteorological and chemical fields suggested that the model system
357 results satisfactorily match the observed data both at ground and upper-air levels. The model results
358 reveal that the O_3 concentrations in Hangzhou were highly relevant to the tropical cyclone in the
359 East China Sea. Throughout the simulation period, large-scale air mass circulations and energy
360 transport by the tropical cyclone probably resulted in a considerably high upper-air O_3-rich mass in
361 the YRD region in both horizontal and vertical scales; this thus engendered a negative background
362 O_3 concentration. As the tropical cyclone approached and hence a prevailing north wind component,
363 Hangzhou experienced strong regional transport from North China, which supplied the precursors
364 to Hangzhou. After or before the tropical cyclone, peripheral downdraft or air subsidence produced
365 stable and calm weather, such as a high pressure and temperature and weak wind, in addition to
366 aggravating the urban heat island effect. These combinations enhanced the chemical generation
367 process and markedly increased the surface O_3 concentrations. Our study provides scientific insight

into urban O_3 formation and dispersion under short-term emission reductions for major events in summer in East China.

Acknowledgments

This work was financially supported by the special funds from the Ministry of Environmental Protection of China (No. 201409008-4) and the Zhejiang Provincial Key Science and Technology Project for Social Development (No. 2014C03025). We thank the US National Oceanic and Atmospheric Administration for its technical support in WRF-Chem modeling. We thank Anhui Institute of Optics and Fine Mechanics, Chinese Academy of Sciences, for providing the LiDAR dataset. High-resolution emission inventories were provided by the Institute of Environmental Science, Shanghai, China, and the official documents of emission control policies were obtained from the Hangzhou Environmental Monitoring Center.

Reference

Browell, E.V., Ismail, S., Grant, W.B., 1998. Differential absorption lidar (DIAL) measurements from air and space. Appl. Phys. B Lasers Opt. 67, 399–410. doi:10.1007/s003400050523

Browell, E. V., 1989. Differential Absorption Lidar Sensing of Ozone. Proc. IEEE 77, 419–432. doi:10.1109/5.24128

Brown, J.F., Loveland, T.R., Merchant, J.W., Reed, B.C., Ohlen, D.O., 1993. Using Multisource Data in Global Land-Cover Characterization - Concepts, Requirements, and Methods. Photogramm. Eng. Remote Sensing 59, 977–987.

Calfapietra, C., Morani, A., Sgrigna, G., Di Giovanni, S., Muzzini, V., Pallozzi, E., Guidolotti, G., Nowak, D., Fares, S., 2016. Removal of Ozone by Urban and Peri-Urban Forests: Evidence from Laboratory, Field, and Modeling Approaches. J. Environ. Qual. 45, 224. doi:10.2134/jeq2015.01.0061

Cheng, W.L., Lai, L.W., Den, W., Wu, M.T., Hsueh, C.A., Lin, P.L., Pai, C.L., Yan, Y.L., 2014. The relationship between typhoons' peripheral circulation and ground-level ozone concentrations in central Taiwan. Environ. Monit. Assess. 186, 791–804. doi:10.1007/s10661-013-3417-7

Emery, C., Tai, E., Yarwood, G., 2001. Enhanced meteorological modeling and performance evaluation for two Texas episodes. International Corp (Ed.), Report to the Texas Natural Resources Conservation Commission, p.b.E (2001) [Novato, CA.]

396 Emmons, L.K., Walters, S., Hess, P.G., Lamarque, J.-F., Pfister, G.G., Fillmore, D., Granier, C., Guenther, A.,
397 Kinnison, D., Laepple, T., Orlando, J., Tie, X., Tyndall, G., Wiedinmyer, C., Baughcum, S.L., Kloster, S.,
398 2010. Description and evaluation of the Model for Ozone and Related chemical Tracers, version 4
399 (MOZART-4). Geosci. Model Dev. 3, 43–67. doi:10.5194/gmd-3-43-2010
400 Friedl, M. ., McIver, D. ., Hodges, J. C. ., Zhang, X. ., Muchoney, D., Strahler, A. ., Woodcock, C. ., Gopal, S.,
401 Schneider, A., Cooper, A., Baccini, A., Gao, F. and Schaaf, C.: Global land cover mapping from MODIS:
402 algorithms and early results, Remote Sens. Environ., 83(12), 287–302, doi:10.1016/S0034-4257(02)00078-0,
403 2002.
404 Gao, J., Zhu, B., Xiao, H., Kang, H., Hou, X., Shao, P., 2016. A case study of surface ozone source apportionment
405 during a high concentration episode, under frequent shifting wind conditions over the Yangtze River Delta,
406 China. Sci. Total Environ. 544, 853–863. doi:10.1016/j.scitotenv.2015.12.039
407 Gonçalves, M., Jiménez-Guerrero, P., Baldasano, J.M., 2009. Contribution of atmospheric processes affecting the
408 dynamics of air pollution in South-Western Europe during a typical summertime photochemical episode.
409 Atmos. Chem. Phys. 9, 849–864. doi:10.5194/acp-9-849-2009
410 Grell, G.A., Peckham, S.E., Schmitz, R., McKeen, S.A., Frost, G., Skamarock, W.C., Eder, B., 2005. Fully coupled
411 “online” chemistry within the WRF model. Atmos. Environ. 39, 6957–6975.
412 doi:10.1016/j.atmosenv.2005.04.027
413 Grell, G., Baklanov, A., 2011. Integrated modeling for forecasting weather and air quality: A call for fully coupled
414 approaches. Atmos. Environ. 45, 6845–6851. doi:10.1016/j.atmosenv.2011.01.017
415 Ha, S., Hu, H., Roussos-Ross, D., Haidong, K., Roth, J., Xu, X., 2014. The effects of air pollution on adverse birth
416 outcomes. Environ. Res. 134, 198–204. doi:10.1016/j.envres.2014.08.002
417 Hsu, J., Prather, M.J., 2014. Is the residual vertical velocity a good proxy for stratosphere-troposphere exchange of
418 ozone? Geophys. Res. Lett. 41, 9024–9032. doi:10.1002/2014GL061994
419 Huang, J.P., Fung, J.C.H., Lau, A.K.H., Qin, Y., 2005. Numerical simulation and process analysis of typhoon-
420 related ozone episodes in Hong Kong. J. Geophys. Res. D Atmos. 110, 1–17. doi:10.1029/2004JD004914
421 Hung, C.H., LouoC, K., 2015. Relationships between Ambient Ozone Concentration Changes in Southwestern
422 Taiwan and Invasion Tracks of Tropical Typhoons. Adv. Meteorol. doi:10.1155/2015/402976
423 Jenkin, M. E., Saunders, S. M. and Pilling, M. J., 1997. The tropospheric degradation of volatile organic
424 compounds: A protocol for mechanism development, Atmos. Environ., 31(1), 81–104, doi:10.1016/S1352-
425 2310(96)00105-7

426 Jiang, F., Zhou, P., Liu, Q., Wang, T., Zhuang, B., Wang, X., 2012. Modeling tropospheric ozone formation over
427 East China in springtime. J. Atmos. Chem. 69, 303–319. doi:10.1007/s10874-012-9244-3
428 Jiang, Y.C., Zhao, T.L., Liu, J., Xu, X.D., Tan, C.H., Cheng, X.H., Bi, X.Y., Gan, J.B., You, J.F., Zhao, S.Z., 2015.
429 Why does surface ozone peak before a typhoon landing in southeast China? Atmos. Chem. Phys. 15, 13331–
430 13338. doi:10.5194/acp-15-13331-2015
431 Jones, S.L., Creighton, G.A., Kuchera, E.L., Rentschler, S.A., 2011. Adapting WRF-CHEM GOCART for Fine-
432 Scale Dust Forecasting, in: AGU Fall Meeting Abstracts. p. 6.
433 Kheirbek, I., Wheeler, K., Walters, S., Kass, D., Matte, T., 2013. PM2.5 and ozone health impacts and disparities
434 in New York City: Sensitivity to spatial and temporal resolution. Air Qual. Atmos. Heal. 6, 473–486.
435 doi:10.1007/s11869-012-0185-4
436 Knote, C., Tuccella, P., Curci, G., Emmons, L., Orlando, J.J., Madronich, S., Baró, R., Jiménez-Guerrero, P.,
437 Luecken, D., Hogrefe, C., Forkel, R., Werhahn, J., Hirtl, M., Pérez, J.L., San José, R., Giordano, L., Brunner,
438 D., Yahya, K., Zhang, Y., 2015. Influence of the choice of gas-phase mechanism on predictions of key
439 gaseous pollutants during the AQMEII phase-2 intercomparison. Atmos. Environ. 115, 553–568.
440 doi:10.1016/j.atmosenv.2014.11.066
441 Lai, L. W. and Cheng, W. L.: Air quality influenced by urban heat island coupled with synoptic weather patterns,
442 Sci. Total Environ., 407(8), 2724–2733, doi:10.1016/j.scitotenv.2008.12.002, 2009.
443 Landry, J.S., Neilson, E.T., Kurz, W.A., Percy, K.E., 2013. The impact of tropospheric ozone on landscape-level
444 merchantable biomass and ecosystem carbon in Canadian forests. Eur. J. For. Res. 132, 71–81.
445 doi:10.1007/s10342-012-0656-z
446 Lelieveld, J., Evans, J.S., Fnais, M., Giannadaki, D., Pozzer, A., 2015. The contribution of outdoor air pollution
447 sources to premature mortality on a global scale. Nature 525, 367–71. doi:10.1038/nature15371
448 Li, M. ., Song, Y. ., Huang, X. ., Li, J. ., Mao, Y. ., Zhu, T. ., Cai, X. . and Liu, B. .: Improving mesoscale modeling
449 using satellite-derived land surface parameters in the Pearl River Delta region, China, J. Geophys. Res.
450 Atmos., 119(11), 6325–6346, doi:10.1002/2014JD021871, 2014.
451 Li, M., Zhang, Q., Kurokawa, J.-I., Woo, J.-H., He, K., Lu, Z., Ohara, T., Song, Y., Streets, D.G., Carmichael, G.R.,
452 Cheng, Y., Hong, C., Huo, H., Jiang, X., Kang, S., Liu, F., Su, H., Zheng, B., 2017. MIX: a mosaic Asian
453 anthropogenic emission inventory under the international collaboration framework of the MICS-Asia and
454 HTAP. Atmos. Chem. Phys. 17, 935–963. doi:10.5194/acp-17-935-2017

455 Lin, M., Fiore, A.M., Cooper, O.R., Horowitz, L.W., Langford, A.O., Levy, H., Johnson, B.J., Naik, V., Oltmans,
456 S.J., Senff, C.J., 2012. Springtime high surface ozone events over the western United States: Quantifying the
457 role of stratospheric intrusions. J. Geophys. Res. Atmos. 117. doi:10.1029/2012JD018151
458 Lin, M., Fiore, A.M., Horowitz, L.W., Langford, A.O., Oltmans, S.J., Tarasick, D., Rieder, H.E., 2015. Climate
459 variability modulates western US ozone air quality in spring via deep stratospheric intrusions. Nat. Commun.
460 6, 7105. doi:10.1038/ncomms8105
461 McNally DE. 12 km MM5 performance goals. Presentation to the Ad-hov Meteorology Group; 2009.
462 Monks, P.S., Archibald, A.T., Colette, A., Cooper, O., Coyle, M., Derwent, R., Fowler, D., Granier, C., Law, K.S.,
463 Mills, G.E., Stevenson, D.S., Tarasova, O., Thouret, V., von Schneidemesser, E., Sommariva, R., Wild, O.,
464 Williams, M.L., 2015. Tropospheric ozone and its precursors from the urban to the global scale from air
465 quality to short-lived climate forcer. Atmos. Chem. Phys. 15, 8889–8973. doi:10.5194/acp-15-8889-2015
466 Nagashima, T., Sudo, K., Akimoto, H., Kurokawa, J., Ohara, T., 2017. Long-term change in the source
467 contribution to surface ozone over Japan. Atmos. Chem. Phys. 17, 8231–8246. doi:10.5194/acp-17-8231-
468 2017
469 Narumi, D., Kondo, A. and Shimoda, Y.: The effect of the increase in urban temperature on the concentration of
470 photochemical oxidants, Atmos. Environ., 43(14), 2348–2359, doi:10.1016/j.atmosenv.2009.01.028, 2009.
471 Ni, Z. zhen, Luo, K., Zhang, J. xi, Feng, R., Zheng, H. xin, Zhu, H. ran, Wang, J. fan, Fan, J. ren, Gao, X. and Cen,
472 K. fa: Assessment of winter air pollution episodes using long-range transport modeling in Hangzhou, China,
473 during World Internet Conference, 2015, in Environmental Pollution, vol. 236, pp. 550–561., 2018.
474 Ortiz, E.E.A.A.G., 2015. Air quality in Europe — 2015 report. Report 1–64. doi:10.2800/62459
475 Paoletti, E., De Marco, A., Beddows, D.C.S., Harrison, R.M., Manning, W.J., 2014. Ozone levels in European and
476 USA cities are increasing more than at rural sites, while peak values are decreasing. Environ. Pollut. 192,
477 295–299. doi:10.1016/j.envpol.2014.04.040
478 Shi, C., Wang, S., Liu, R., Zhou, R., Li, D., Wang, W., Li, Z., Cheng, T., Zhou, B., 2015. A study of aerosol optical
479 properties during ozone pollution episodes in 2013 over Shanghai, China. Atmos. Res. 153, 235–249.
480 doi:10.1016/j.atmosres.2014.09.002
481 Shu, L., Xie, M., Wang, T., Chen, P., Han, Y., Li, S., Zhuang, B., Li, M., Gao, D., 2016. Integrated studies of a
482 regional ozone pollution synthetically affected by subtropical high and typhoon system in the Yangtze River
483 Delta region, China. Atmos. Chem. Phys. Discuss. 0, 1–32. doi:10.5194/acp-2016-581

484 Sillman, S.: The relation between ozone, NO(x) and hydrocarbons in urban and polluted rural environments,
485 Atmos. Environ., 33(12), 1821–1845, doi:10.1016/S1352-2310(98)00345-8, 1999.
486 Stauffer, D.R., Seaman, N.L., Binkowski, F.S., 1991. Use of Four-Dimensional Data Assimilation in a Limited-
487 Area Mesoscale Model Part II: Effects of Data Assimilation within the Planetary Boundary Layer. Mon.
488 Weather Rev. doi:10.1175/1520-0493(1991)119<0734:UOFDDA>2.0.CO;2
489 Su, W., Liu, C., Hu, Q., Fan, G., Xie, Z., Huang, X., Zhang, T., Chen, Z., Dong, Y., Ji, X., Liu, H., Wang, Z., Liu,
490 J., 2017. Characterization of ozone in the lower troposphere during the 2016 G20 conference in Hangzhou.
491 Sci. Rep. 7, 17368. doi:10.1038/s41598-017-17646-x
492 Tang, G., Li, X., Wang, Y., Xin, J., Ren, X., 2009. Surface ozone trend details and interpretations in Beijing , 2001
493 – 2006. Atmos. Chem. Phys. 8813–8823. doi:10.5194/acpd-9-8159-2009
494 Tang, G., Wang, Y., Li, X., Ji, D., Hsu, S., Gao, X., 2012. Spatial-temporal variations in surface ozone in Northern
495 China as observed during 2009-2010 and possible implications for future air quality control strategies.
496 Atmos. Chem. Phys. 12, 2757–2776. doi:10.5194/acp-12-2757-2012
497 Tang, G., Zhu, X., Xin, J., Hu, B., Song, T., Sun, Y., Wang, L., Cheng, M., Li, X., Wang, Y., Zhang, J., Chao, N.,
498 Kong, L., Li, X., 2017a. Modelling study of boundary-layer ozone over northern China - Part I: Ozone
499 budget in summer. Atmos. Res. 187, 128–137. doi:10.1016/j.atmosres.2016.10.017
500 Tang, Q., Prather, M.J., Hsu, J., 2011. Stratosphere-troposphere exchange ozone flux related to deep convection.
501 Geophys. Res. Lett. 38. doi:10.1029/2010GL046039
502 Teixeira, E., Fischer, G., van Velthuizen, H., van Dingenen, R., Dentener, F., Mills, G., Walter, C., Ewert, F., 2011.
503 Limited potential of crop management for mitigating surface ozone impacts on global food supply. Atmos.
504 Environ. 45, 2569–2576. doi:10.1016/j.atmosenv.2011.02.002
505 Tie, X., Geng, F., Guenther, A., Cao, J., Greenberg, J., Zhang, R., Apel, E., Li, G., Weinheimer, A., Chen, J., Cai,
506 C., 2013. Megacity impacts on regional ozone formation: Observations and WRF-Chem modeling for the
507 MIRAGE-Shanghai field campaign. Atmos. Chem. Phys. 13, 5655–5669. doi:10.5194/acp-13-5655-2013
508 Tuccella, P., Curci, G., Visconti, G., Bessagnet, B., Menut, L., Park, R.J., 2012. Modeling of gas and aerosol with
509 WRF/Chem over Europe: Evaluation and sensitivity study. J. Geophys. Res. Atmos. 117.
510 doi:10.1029/2011JD016302
511 USEPA: Guidance on the Use of Models and Other Analyses for Demonstrating Attainment of Air Quality Goals
512 for Ozone, PM2.5 and Regional Haze, EPA-454/B-07e002. USEPA, 2007

513 von Schneidemesser, E., Coates, J., Denier van der Gon, H.A.C., Visschedijk, A.J.H., Butler, T.M., 2016. Variation
514 of the NMVOC speciation in the solvent sector and the sensitivity of modelled tropospheric ozone. Atmos.
515 Environ. 135, 59–72. doi:10.1016/j.atmosenv.2016.03.057
516 Walcek, C. J., Yuan, H.-H., Walcek, C. J. and Yuan, H.-H.: Calculated Influence of Temperature-Related Factors
517 on Ozone Formation Rates in the Lower Troposphere, J. Appl. Meteorol., 34(5), 1056–1069,
518 doi:10.1175/1520-0450(1995)034<1056:CIOTRF>2.0.CO;2, 1995.
519 Wang, S., Xing, J., Chatani, S., Hao, J., Klimont, Z., Cofala, J., Amann, M., 2011. Verification of anthropogenic
520 emissions of China by satellite and ground observations. Atmos. Environ. 45, 6347–6358.
521 doi:10.1016/j.atmosenv.2011.08.054
522 Wang, T.J., Lam, K.S., Xie, M., Wang, X.M., Carmichael, G., Li, Y.S., 2006. Integrated studies of a photochemical
523 smog episode in Hong Kong and regional transport in the Pearl River Delta of China. Tellus, Ser. B Chem.
524 Phys. Meteorol. 58, 31–40. doi:10.1111/j.1600-0889.2005.00172.x
525 Wang, T., Xue, L., Brimblecombe, P., Lam, Y. F., Li, L. and Zhang, L.: Ozone pollution in China: A review of
526 concentrations, meteorological influences, chemical precursors, and effects, Sci. Total Environ., 575, 1582–
527 1596, doi:10.1016/j.scitotenv.2016.10.081, 2017.
528 Wang, Y., Hu, B., Tang, G., Ji, D., Zhang, H., Bai, J., Wang, X., Wang, Y., 2013. Characteristics of ozone and its
529 precursors in Northern China: A comparative study of three sites. Atmos. Res. 132–133, 450–459.
530 doi:10.1016/j.atmosres.2013.04.005
531 Wang, Y.H., Hu, B., Ji, D.S., Liu, Z.R., Tang, G.Q., Xin, J.Y., Zhang, H.X., Song, T., Wang, L.L., Gao, W.K.,
532 Wang, X.K., Wang, Y.S., 2014. Ozone weekend effects in the Beijing-Tianjin-Hebei metropolitan area,
533 China. Atmos. Chem. Phys. 14, 2419–2429. doi:10.5194/acp-14-2419-2014
534 Wilson, R.C., Fleming, Z.L., Monks, P.S., Clain, G., Henne, S., Konovalov, I.B., Szopa, S., Menut, L., 2012. Have
535 primary emission reduction measures reduced ozone across Europe? An analysis of European rural
536 background ozone trends 1996-2005. Atmos. Chem. Phys. 12, 437–454. doi:10.5194/acp-12-437-2012
537 Xie, M., Zhu, K., Wang, T., Yang, H., Zhuang, B., Li, S., Li, M., Zhu, X., Ouyang, Y., 2014. Application of
538 photochemical indicators to evaluate ozone nonlinear chemistry and pollution control countermeasure in
539 China. Atmos. Environ. 99, 466–473. doi:10.1016/j.atmosenv.2014.10.013
540 Xing, C., Liu, C., Wang, S., Lok Chan, K., Gao, Y., Huang, X., Su, W., Zhang, C., Dong, Y., Fan, G., Zhang, T.,
541 Chen, Z., Hu, Q., Su, H., Xie, Z., Liu, J., 2017. Observations of the vertical distributions of summertime

atmospheric pollutants and the corresponding ozone production in Shanghai, China. Atmos. Chem. Phys. 17, 14275–14289. doi:10.5194/acp-17-14275-2017

Xue, L.K., Wang, T., Gao, J., Ding, A.J., Zhou, X.H., Blake, D.R., Wang, X.F., Saunders, S.M., Fan, S.J., Zuo, H.C., Zhang, Q.Z., Wang, W.X., 2014. Ground-level ozone in four Chinese cities: Precursors, regional transport and heterogeneous processes. Atmos. Chem. Phys. 14, 13175–13188. doi:10.5194/acp-14-13175-2014

Zhang, B.N., Kim Oanh, N.T., 2002. Photochemical smog pollution in the Bangkok Metropolitan Region of Thailand in relation to O3 precursor concentrations and meteorological conditions. Atmos. Environ. 36, 4211–4222. doi:10.1016/S1352-2310(02)00348-5

Zhang, H., Chen, G., Hu, J., Chen, S.H., Wiedinmyer, C., Kleeman, M., Ying, Q., 2014. Evaluation of a seven-year air quality simulation using the Weather Research and Forecasting (WRF)/Community Multiscale Air Quality (CMAQ) models in the eastern United States. Sci. Total Environ. 473–474, 275–285. doi:10.1016/j.scitotenv.2013.11.121

Zhang, Y., Zhang, X., Wang, L., Zhang, Q., Duan, F., He, K., 2016. Application of WRF/Chem over East Asia: Part I. Model evaluation and intercomparison with MM5/CMAQ. Atmos. Environ. 124, 285–300. doi:10.1016/j.atmosenv.2015.07.022

Zhang, Y.H., Su, H., Zhong, L.J., Cheng, Y.F., Zeng, L.M., Wang, X.S., Xiang, Y.R., Wang, J.L., Gao, D.F., Shao, M., Fan, S.J., Liu, S.C., 2008. Regional ozone pollution and observation-based approach for analyzing ozone-precursor relationship during the PRIDE-PRD2004 campaign. Atmos. Environ. 42, 6203–6218. doi:10.1016/j.atmosenv.2008.05.002